Nanoscale

PAPER

View Article Online
View Journal | View Issue

Cite this: *Nanoscale*, 2019, **11**, 19842

Nanocellulose/bioactive glass cryogels as scaffolds for bone regeneration†

Filipe V. Ferreira, *[a,b,c,d] Lucas P. Souza,[e] Thais M. M. Martins,[f] João H. Lopes,[g] Bruno D. Mattos,[c] Marcos Mariano,[b] Ivanei F. Pinheiro,[a,b] Thalita M. Valverde,[h] Sébastien Livi,[d] José A. Camilli,[e] Alfredo M. Goes,[i] Rubia F. Gouveia,[b] Liliane M. F. Lona[a] and Orlando J. Rojas *[c]

A major challenge exists in the preparation of scaffolds for bone regeneration, namely, achieving simultaneously bioactivity, biocompatibility, mechanical performance and simple manufacturing. Here, cellulose nanofibrils (CNF) are introduced for the preparation of scaffolds taking advantage of their biocompatibility and ability to form strong 3D porous networks from aqueous suspensions. CNF are made bioactive for bone formation through a simple and scalable strategy that achieves highly interconnected 3D networks. The resultant materials optimally combine morphological and mechanical features and facilitate hydroxyapatite formation while releasing essential ions for *in vivo* bone repair. The porosity and roughness of the scaffolds favor several cell functions while the ions act in the expression of genes associated with cell differentiation. Ion release is found critical to enhance the production of the bone morphogenetic protein 2 (BMP-2) from cells within the fractured area, thus accelerating the *in vivo* bone repair. Systemic biocompatibility indicates no negative effects on vital organs such as the liver and kidneys. The results pave the way towards a facile preparation of advanced, high performance CNF-based scaffolds for bone tissue engineering.

Received 25th June 2019,
Accepted 14th August 2019

DOI: 10.1039/c9nr05383b

rsc.li/nanoscale

Introduction

Tissue engineering has allowed the introduction of functional constructs for the regeneration of defective or lost biological tissues.[1,2] Recent efforts have showed that three-dimensional, highly porous polymer scaffolds are suitable to promote cell functions, and consequently tissue regeneration.[3–5] Specifically, practical implementation of such materials for bone formation may involve the seeding of the patient's own cells within the scaffold, before implantation, or placing the scaffold directly in the fracture (damaged) area to promote proliferation of cells and *in vivo* growth.[6,7] Regardless of the approach employed, the scaffolds are of critical importance since they directly affect the attachment, differentiation and maturation of cells as well as matrix formation for their survival. Scaffolds must display high porosity and rough surfaces combined with the necessary mechanical strength to support the cells and to match the performance of the tissues at the site of implantation. Additionally, they must bond chemically with tissue.[8]

The design of scaffolds that combine the above-mentioned characteristics can be achieved by "soft matter" engineering. This has inspired recent research efforts for the preparation of scaffolds from polymers[9–12] and bio-based colloids[13–15] that can be implemented in surgical procedures. In this respect, nanocellulose presents a unique set of properties that includes flexibility, mechanical strength and biocompatibility.[16–20] In fact, nanocellulose-based aero- and cryogels meet the microstructure and mechanical performance requirements of scaffolds for tissue engineering.[21] However, for use as bone

[a]*School of Chemical Engineering, University of Campinas (UNICAMP), 13083-970 Campinas-SP, Brazil. E-mail: filipevargasf@gmail.com*
[b]*Brazilian Nanotechnology National Laboratory (LNNano), Brazilian Center for Research in Energy and Materials (CNPEM), 13083-970 Campinas-SP, Brazil*
[c]*Department of Bioproducts and Biosystems, Aalto University School of Chemical Engineering, P.O. Box 16300, 00076, Aalto University, Finland. E-mail: orlando.rojas@aalto.fi*
[d]*Université de Lyon, Ingénierie des Matériaux Polymères CNRS, UMR 5223, INSA Lyon, F-69621 Villeurbanne, France*
[e]*Department of Structural and Functional Biology, Institute of Biology, University of Campinas (UNICAMP), 13083-862 Campinas-SP, Brazil*
[f]*Department of Morphology, Institute of Biological Sciences, Federal University of Minas Gerais (UFMG), 31270-901 Belo Horizonte-MG, Brazil*
[g]*Department of Chemistry, Division of Fundamental Sciences (IEF), Technological Institute of Aeronautics (ITA), 12228-900 Sao Jose dos Campos-SP, Brazil*
[h]*Department of Biochemistry and Immunology, Institute of Biological Sciences, Federal University of Minas Gerais (UFMG), 31270-901 Belo Horizonte-MG, Brazil*
[i]*Department of Pathology, Institute of Biological Sciences, Federal University of Minas Gerais (UFMG), 31270-901 Belo Horizonte-MG, Brazil*

†Electronic supplementary information (ESI) available: Experimental section and supplementary discussion. See DOI: 10.1039/c9nr05383b

tissue, a limiting factor in nanocellulose utilization is the lack of bioactivity to induce bone regeneration. A recent effort used cellulose nanocrystal (CNC) aerogels to facilitate *in vivo* formation of bone.[22] Here, we propose cellulose nanofibrils (CNF), which effectively form networks in composites, to form porous macrostructures that are able to grow and regenerate bone by the addition of bioactive glass.[23,24] Thus, the high mechanical performance of the cellulose nanostructures is combined with the bioactivity of the mineral component (containing SiO_2, CaO, Na_2O, and P_2O) to form an advanced biomedical composite. This strategy overcomes the two main obstacles found in the individual use of these materials for bone tissue engineering, namely, the absence of bioactivity in nanocellulose and the brittleness of the bioactive glass and the challenges it poses in manufacturing complex structures. We exploit the synergies of such organic–inorganic composites, in which the cellulose nanofibrils act as a morphological guide for nucleation and further biomineralization *via* reactions involving the mineral phase of the bioactive glass in contact with the physiological fluids. It is expected that the glass phase not only allows the formation of hydroxyapatite layers on the fibrils, favoring cell attachment, but also induces the leaching of ions that are key to activate the expression of osteogenic genes[25,26] and stimulate angiogenesis.[27–30]

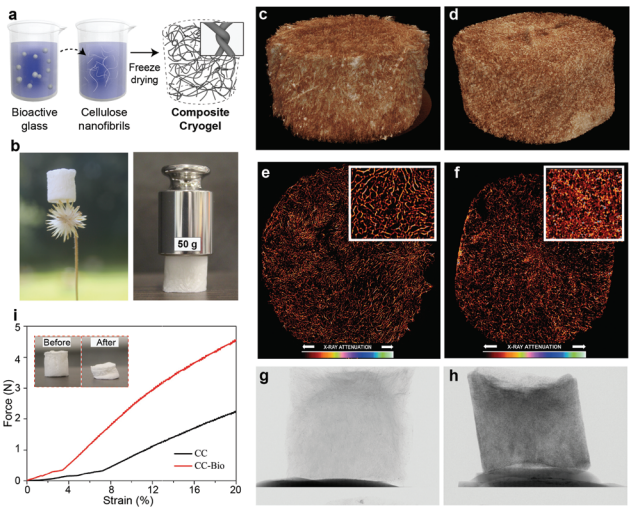

Fig. 1 (a) Schematic illustration of the preparation of composite cellulose-based cryogels, CC-Bio, with the inset showing the characteristic entangled contact points of CNF networks. (b) Photographs of CC-Bio showing its characteristic light weight and high strength. X-ray microtomography images of (c and d) 3D reconstruction and (e and f) 2D slices taken from the 3D images and their respective (g and h) X-ray projections. The images c, e, and g correspond to the pure cellulose cryogel (CC), while d, f, and h correspond to the composite cryogel (CC-Bio). (i) Force–strain profiles obtained after the uniaxial compression of CC and CC-Bio (the inset corresponds to the photographs of CC-Bio before and after compression).

Results and discussion

The herein proposed scaffolds were prepared, without the need for crosslinking, through a straightforward freeze-casting protocol of colloidal aqueous suspensions of CNF containing dispersed bioactive glass (Fig. 1a). A composite cryogel comprising *ca.* 80 wt% (dry basis) bioactive glass and 20 wt% (dry basis) CNF, referred to as CC-Bio, is shown in Fig. S1.† Although chiefly made up of brittle and fragile bioglass, the composite cryogels preserve the intrinsic mouldable, characteristics of CNF hydrogels and cryogels even after biomineralization. The highly porous, interconnected structure of the cryogels, a paramount characteristic in scaffold design, is evidenced by high-resolution X-ray micro-computed tomography (μCT) imaging. We further discuss the formation of hydroxyapatite layers upon contact with simulated body fluid (SBF), the kinetics of ion release from the composite cryogels, and their cytocompatibility, putting emphasis on the importance of these features for cell differentiation and bone formation. Additionally, we perform *in vivo* tests using rat calvarial defect models to provide a practical demonstration of the application of the composite scaffolds in living organisms. Lastly, we show that the obtained scaffolds do not negatively affect vital organs such as the kidneys and liver.

The composite CC-Bio cryogels, comprising an optimized bioactive glass loading (see ESI Discussion S1 and Fig. S1†), presented low density and extremely high strength, resisting compressive loads over 1250 times their own weight (Fig. 1b). The nanofibrils contributed with their highly percolated assemblies that go beyond classical orthogonal contacts that otherwise take place with stiff building blocks.[31] We compared, by μCT imaging, the morphology of CC-Bio to that of cryogels prepared with monolithic CNF, further referred to as CC. Even if added at low mass fractions, CNF provided a framework for the cryogel to form, owing to the highly entangled fibrils.[32] This led to freeze-cast porous structures that corresponded to classical cellular materials ($E \sim \rho^2$), similar to human bones.[33] 2D slices of the micro-tomograms (Fig. 1e and f) highlight CC and CC-Bio cryogels with similar morphological features, namely, porous networks interconnected by macroscopic channels. These architectures are expected to favor the infiltration of blood vessels, cell migration, and nutrient transport.[34] From the quantitative morphological evaluation, it was confirmed that the bioactive glass was deposited onto the surface of the fibrils, leading to increased pore wall thickness from 33 ± 8 to 45 ± 11 μm (ESI Discussion S2†). Therefore, lower densities of interlayer pores and smaller pores were observed (Fig. S2†). Large pores were apparent for CC (140 ± 44 μm) and CC-Bio (135 ± 33 μm) (Fig. S3†), suitable for adhesion and proliferation of osteoblasts without cell aggregation[35] and proper scaffold vascularization.[36] The relatively smaller pores in CC-Bio influenced the stress–strain profiles obtained from the uniaxial compression of the cryogels (Fig. 1i and Fig. S1†), which revealed a plastic regime for CC and CC-Bio that was initiated at strains of *ca.* 3.5 and 7%, respectively. The elastic regime of cellulose-based cellular materials correlated with their porosity.[21] Increased cryogel compression strength, from 11 ± 1 to 24 ± 1 kPa, was

noted with the increased wall thickness (by almost 40%), yielding a flexible, yet strong material (Fig. 1i). These features match those of tissues for targeted implantation sites, which are rigid but not fragile. Importantly, the mechanical performance of the cryogels was evaluated under dry conditions, which is important as far as implantation and early performance are concerned. However, wet and cycled wet/dry conditions may change the mechanical performance of the materials. This has been partially discussed for cryogels prepared from CNC, which showed a near 2-fold decrease in compression strength after three wet cyclic measurements.[22] Additionally, in our recent report we investigated the compressive strength organic–inorganic composite materials (SiO_2/CNF) under several harsh conditions.[37] We showed that the mechanical performance of the composites decreased under wet conditions, but they remained similar after 5 wetting-drying cycles. It is reasonable to expect that the CNF/bioactive glass materials prepared herein behave similarly.

The prepared cryogels were exposed to SBF, revealing a drastically different behavior as far as hydroxyapatite formation is concerned (Fig. 2). First, we compared the Fourier-transform infrared (FTIR) spectra of pure CNF cryogels (CC), pure bioactive glass, and composite cryogels (CC-Bio) before and after immersion in SBF (see ESI Discussion S3†). The CC-Bio cryogels displayed extensive formation of carbonated apatite layers, as can be concluded from the increased signal of crosslinked ≡Si–O–Si≡ at 1030 cm^{-1} and the reduction of the Si-NBO, non-bridging oxygen absorption. Such effects are related to the formation of a silica gel layer on the fibrils and the partial dissolution of the bioactive glass, which occurs by ion exchange of Ca^{2+} and Na^{+} from the mineral network with H_3O^{+} from the SBF solution.[24] Furthermore, hydroxyapatite formation was confirmed by X-ray photoelectron spectroscopy (XPS; ESI Discussion S4 and Fig. S4–S7†). Principally, the formation of the apatite layer was verified by the significant changes in the relative concentration of P and Ca species on the surface of CC-Bio after immersion in SBF. These changes only occurred for the cryogel containing bioactive glass. Furthermore, scanning electron microcopy (SEM) images (Fig. 2b–e) revealed the typical "cauliflower" morphology of hydroxyapatite, only observed in CC-Bio (Fig. 2e) upon immersion in SBF. The CNF framework was coated with hydroxyapatite, resulting in mineralized architectures with rough and less-ordered structures. The apatite layer is chemically and structurally equivalent to the mineral phase in bone, which improves the interfacial bonding between the scaffolds and bone tissues.[38] Additionally, the inherent rough surface of the apatite layer favors key cell functions in bone tissue engineering.

Another important aspect for bone tissue application is the release of ions, which activates the expression of the osteogenic genes[25] and stimulates angiogenesis.[27] Angiogenesis is of critical importance in tissue regeneration.[39,40] The improvement of vascularization allows gas exchange and nutrient transport to osteoblast cells, which are needed for repair of large bone defects.[41,42] Moreover, angiogenesis may lead to the recruitment of stem cells to the injured site and their orientation to the osteoblastic lineage.[43] In this context, scaffolds play an important role, especially in adequate vascularization at the defect site and consequently in bone regeneration.[44] It has been demonstrated that 30–40 μm is the minimum porosity required for gas exchange and nutrient transport in the scaffold through the blood vessel.[45] A pore size of about 160–270 μm has been reported to facilitate neovascularization.[46] Several strategies to promote angiogenesis have been developed to support the successful treatment of large bone defects,[47,48] including treatment using different ions.[27–30] Although not fully investigated, we suggest that the CNF/bioactive glass addresses aspects related to the structure–biology relationship.

The cellulosic framework, by itself, is not a source of ions, making it mandatory the use of an additional phase, in this case the bioactive glass, for effective bone regeneration. We used inductively coupled plasma (ICP) spectroscopy to quantitatively assess the dissolution products of the CC-Bio cryogel during immersion in HEPES solution (Fig. 2f). The characteristic cascade of events involving the bioactive glass was confirmed, in line with the events described by Hench, who studied the mechanisms for biomineralization.[49] The Na^{+} and Ca^{2+} release profiles plateaued after 720 min at 363 ± 13 and 214 ± 1 ppm, respectively. This behavior suggests the maintenance of the vitreous structure of the mineral phase in the cryogel, *i.e.*, a rapid exchange occurred between Na^{+}/Ca^{2+} from the glass network and H_3O^{+} from solution, which is ascribed to the partial surface dissolution of the bioactive glass. The subsequent biomineralization implies the loss of soluble silica and the formation of SiO_2-rich layers, acting as nucleation centers for the apatite phase. The formation of the silica gel layer and the solubilization of the glassy phase present in the

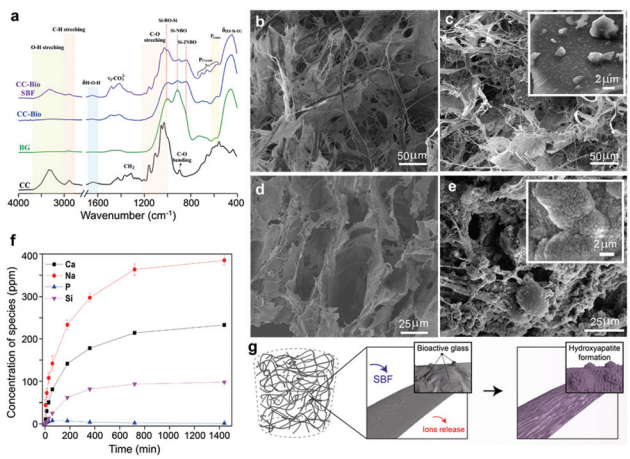

Fig. 2 (a) FTIR spectra of CC and CC-Bio before and after immersion in simulated body fluid (SBF) for 7 days. The FTIR spectrum of the pure bioactive glass was added for comparison purposes. (b–e) Scanning electron micrographs of (b and d) CC and (c and e) CC-Bio. The images show the behavior of the samples (b, c) before and (d, e) after 24 h after immersion in complete culture medium. (f) Release profiles of Ca, Na, P and Si ions from CC-Bio in HEPES solution at pH 7.40. Na, Ca, Si or P species were detected in the case of CC. (g) Schematic illustration showing fibrils with increasingly rough and bioactive hydroxyapatite after contact with SBF.

CC-Bio, as assessed by FTIR and XPS, relate to the leaching of the silicon species. The Si leaching exhibited a similar trend to that displayed for the release of sodium and calcium ions, with a plateau at 93 ± 1 ppm. The release profile of phosphorus peaked after 1 h of immersion, displaying a maximum concentration of 7.89 ± 0.03 ppm (approximately the solubility limit), followed by a dramatic reduction associated with the precipitation of phosphate species in the form of calcium phosphate on the surface of CC-Bio.

The *in vitro* osteogenic ability of the cryogels was evaluated (Fig. 3). Red stained biomineralized nodules, which correspond to the extracellular matrix rich in calcium, were only observed for cells cultured in the presence of CC-Bio (Fig. 3c and d). Such calcium deposits are related to the increase of the alkaline phosphatase (ALP) mRNA expression that is usually followed by an increase in the bone sialoprotein (BSP) gene expression.[50,51] BSP is tightly associated with bone mineralization.[52] The CC-Bio composite cryogels performed better as far as osteogenesis is concerned because of the release of Si, Ca, P, and Na ions from the mineral phase. This greatly enhances the expression of the genes associated with the osteoblast proliferation and differentiation during the formation of the bone extracellular matrix, thus favoring cell differentiation.[53] *In vitro* biocompatibility studies (Fig. S7†) revealed that none of the cryogels significantly affected the metabolic activity and growth of cells; therefore, they can be considered cytocompatible. This is paramount for practical implementations as any sign of toxicity represents a risk for the recipient organism.

So far, hydroxyapatite (HA) layers have been shown to build on virtually any surface,[54–56] but their presence does not guarantee that the material efficiently regenerates bone tissues.[6] An efficient scaffold for bone tissue engineering must combine the formation of HA with biocompatibility, high porosity, mechanical support suitable for cell functions, controlled release of angiogenic agents (ions/species) and ability to stimulate bone differentiation.[57,58] The composite cryogel, CC-Bio, covered all of the above-mentioned requirements to act as a scaffold for *in vivo* bone formation. The aforementioned features encouraged us to investigate the *in vivo* bone regeneration using the rat calvarial defect assay.[59] We prepared cryogels with a diameter and thickness of 5 and 1 mm, respectively. A calvarial defect of 5 mm was then created and the cryogels were placed into the defect site (Fig. 4a). The bare calvarial defect was used as the control. The calvarial bone of the rats was analyzed by μCT after 56 days of scaffold implantation, revealing substantial bone formation for rats implanted with the CC-Bio cryogel (Fig. 4d and g). The bone regeneration reported for the treatment with CC-Bio reached level 3 in the scale described by Patel *et al.*[60] In this guide, a numeric ranking of 0 means no bone formation within the defect area, whereas 4 means bone bridging entirely through the defect at the longest point. We observed that the length of the defect was partially regenerated in 56 days when using the CC-Bio cryogel as the scaffold. Quantitative results acquired from the μCT images (Fig. 4g) showed that a material with the same X-ray attenuation of the surroundings calvarial bone was formed within the CC-Bio cryogel (Fig. 4h). The formed tissue had a higher local density and lower porosity, suggesting the formation of bone within the composite scaffold.

Treatment of large bone defects requires a material with 3D porous architecture and a robust biological activity, offering a

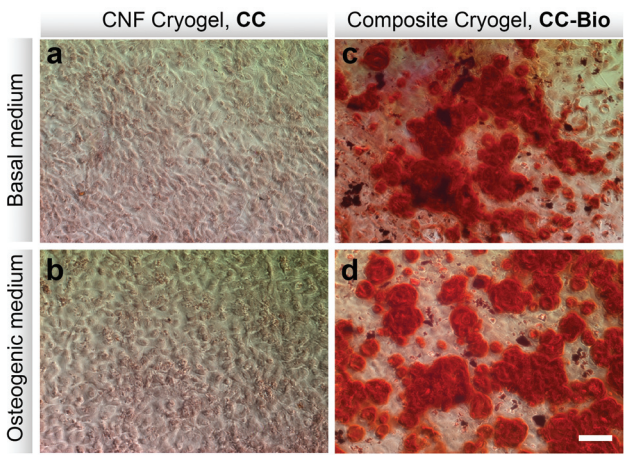

Fig. 3 Mineralization assay with Alizarin Red staining of MC3T3-E1 cells cultured in the presence of (a and b) CC and (c and d) CC-Bio. Mineralization was visualized in cells cultured in the presence of CC-Bio with basal (c) and osteogenic (d) media, but not in cells cultivated in the presence of CC. Scale bar: 200 μm.

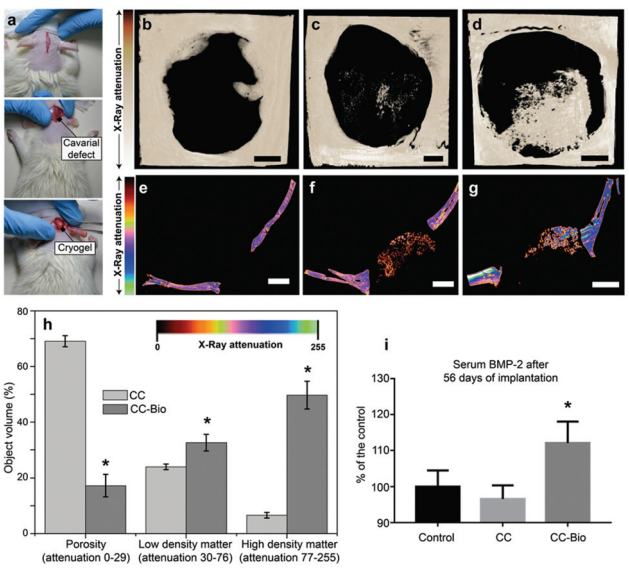

Fig. 4 Evaluation of the *in vivo* performance of the cryogels as far as bone formation is concerned. (a) Photographs of the procedure followed in the rat calvarial assay. Note: The *in vivo* experiments were approved by the Ethics Research Committee of the University of Campinas. (b–g) Representative μCT images of rat calvarial after 56 days of implantation. 3D reconstruction (top row) and 2D slices inside the 3D image (bottom row). (b and e) Control, (c and f) CC and (d and g) CC-Bio. Scale bar represents 1 mm. (h) Quantitative results obtained from μCT imaging of rat calvarial (n = 6). (i) Quantification of serum BMP-2 expressed as a percentage of the control group. * means statistically different by Tukey's test with a significance level of 5%.

suitable niche for regeneration. The remarkable performance, as far as bone regeneration is concerned, observed in CC-Bio, arises from the combined hydroxyapatite growth on the cryogel and the release of the ions from the bioactive glass.[61] The biomineralized cellulose nanofibrils, from HA deposition, are shown to possess a porous and rough morphology (Fig. 2e and g) that favored the adhesion of multipotent cells, which further underwent osteogenic differentiation. Smooth surfaces typically stimulate fibroblastic differentiation of multipotent cells with further production of type I collagen-rich, fibrous, connective tissue membranes. In contrast, rough surfaces, similar to the ones found in the CC-Bio, stimulate differentiation into the osteoblastic lineage and bone formation.[62,63] The ion release stimulates cell differentiation and therefore also induces better bone regeneration. It is known that limited blood supply leads to low bone tissue repair/regeneration and/or to cell death.[40,64–66] This is relevant to angiogenesis, an issue that was not considered. However, given the expected blood transport and availability promoted by the composite, adequate vascularization at the defect site is anticipated, as shown later.

The interaction between the bioactive glass and the surrounding environment (body fluid) also affects cell behavior.[67,68] As discussed earlier, the dissolution products from the bioactive glass are expected to stimulate the proliferation of osteoblasts, inducing insulin-like growth factor II mRNA expression and protein synthesis.[25] The specific ions released from our proposed material may stimulate over 5-fold genes related to cell proliferation and osteogenic differentiation.[53] We measured the behavior of one of the most important proteins for bone formation, the bone morphogenetic protein 2 (BMP-2).[69] The results demonstrated an increase by 12% of BMP-2 after 56 days of implantation of CC-Bio in serum (Fig. 4i), which relates to enhanced bone regeneration. The control and CC counterparts behaved similarly. The BMP-2 protein plays an essential role in the formation of a postnatal skeleton, participating directly in the progression from osteoprogenitor cells to osteocytes through the regulation of Runx2 expression.[69,70] Moreover, it has been successfully used to aid the treatment of non-unions.[70,71] However, there is a concern regarding its ideal administration conditions. A careful evaluation of its dosage is needed as BMP-2 has an anabolic effect on bone, *i.e.*, high doses can promote or worsen bone cancer.[71] Compared to the control group, the results indicated that CC-Bio promoted sufficient endogenous release of BMP-2 to stimulate greater bone formation, with no need of exogenous therapy, reducing the risk of overdose exposure that is inherent to this type of treatment.

Lastly, we thoroughly evaluated the systemic biocompatibility of CC and CC-Bio implants by quantifying the key blood biochemical markers of toxicity from the liver (TGO – glutamic oxaloacetic transaminase and TGP – glutamic pyruvic transaminase; Fig. 5a and b) and kidneys (creatinine; Fig. 5c). Histopathological analyses of the recipient's liver and kidneys were also performed in order to search for any sign of tissue damage caused by possible sub-products of the implants

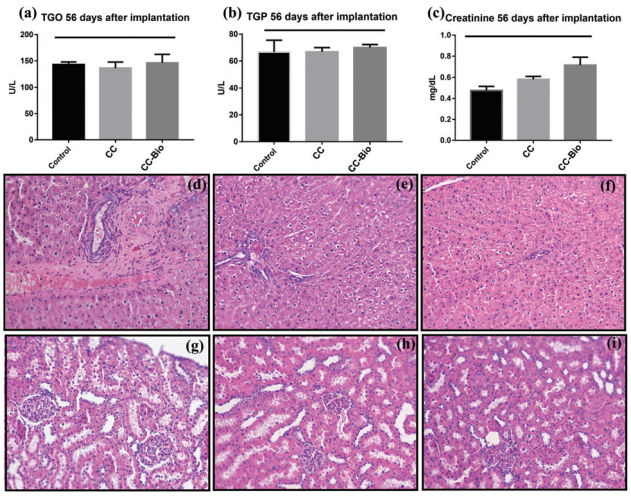

Fig. 5 (a–c) Concentration of the biochemical markers of hepatic and renal damage after 56 postoperative days (n = 6). Data are displayed as mean and SD. One-way ANOVA and Tukey's post-test were performed to compare the experimental and the control groups – no significant difference was found. Photomicrographs of histological sections of the (d–f) liver and (g–i) kidneys of rats from the control (d and g), CC (e and h) and CC-Bio (f and i) groups after 56 postoperative days. Magnification 200×. Haematoxylin and eosin staining. No signs of damage were observed in any of the analyzed organs. These results reveal that the implants were nontoxic to these organs.

(Fig. 5d–i). The results showed the same levels for the markers from the control and the cryogels; moreover, no damage was observed in the organ's tissue, revealing that the implants were nontoxic to metabolic and excretory organs such as the liver and kidneys.

Conclusion

Material advances for the treatment of large bone defects have included ceramics[72] and polymers.[73] The inherent brittleness of the former and low osteo-conductivity of the latter may limit their separate use, for example, for treatment of calvarial defects.[41] Thus, we propose composites based on nanocellulose/bioactive glass, which optimally combine the features needed for bone repair. Moreover, the synthesis of such biomaterials is simple and brings many advantages over the current strategies, which involve solvent-based, chemical cross-linking, multi-step fabrication.[15,74] We show freeze-casting as a facile, green, and scalable approach to achieve light, strong, and highly interconnected bioactive 3D materials for utilization *in vivo*. Moreover, with the recent advances in 3D bioprinting techniques and additive manufacturing for cellulose nanostructures,[75] the proposed materials can be easily shaped in any desired form.

The high porosity of the CC-Bio material and its high specific surface area with high bioactive glass loading prevent extensive adhesion to the organic support, avoiding erosion or dispersion in the blood stream. The mineral phase of CC-Bio

promotes the release of ions (Si, Ca, P, and Na) while, simultaneously, forming rough hydroxyapatite layers upon contact with body fluids. The combination of high porosity, hydroxyapatite formation, and ion release directly affects cell differentiation as well as increases the release of BMP-2 from the cells within fractured sections, greatly improving bone formation. In conclusion, we successfully demonstrated the proposed strategies by using tests *in vitro* and *in vivo*. They show that light-weight, robust, biocompatible, and bioactive cryogels comprising cellulose nanofibrils and bioactive glass fit the requirements of scaffolds for bone tissue engineering.

Experimental part

Experimental part is described in the ESI.†

Conflicts of interest

There are no conflicts to declare.

Acknowledgements

We are very grateful to Professor Celso Aparecido Bertran and Dr Caio Gomide Otoni for their contributions. The authors acknowledge São Paulo Research Foundation – FAPESP (Grant, 2016/09588-9, 2018/16851-3 and 2018/12831-8 – Ph.D. fellowship of F. V. F; 2010/05394-9), CAPES and CNPq for financial support. O. J. R., B. D. M. and F. V. F also acknowledge support from the European Research Council (ERC) under the European Union's Horizon 2020 research and innovation programme (ERC Advanced Grant agreement No 788489, "BioElCell"). The authors thank the LNNano for technical support during μCT, SEM and XPS analyses. The Center of Microscopy at the Federal University of Minas Gerais is acknowledged for providing instrumental and technical support in electron microscopy experiments.

References

1 A. Nasajpour, S. Ansari, C. Rinoldi, A. S. Rad, T. Aghaloo, S. R. Shin, Y. K. Mishra, R. Adelung, W. Swieszkowski, N. Annabi, A. Khademhosseini, A. Moshaverinia and A. Tamayol, *Adv. Funct. Mater.*, 2018, **28**, 1703437.
2 M. P. Lutolf and J. A. Hubbell, *Nat. Biotechnol.*, 2005, **23**, 47–55.
3 M. M. Stevens, *Mater. Today*, 2008, **11**, 18–25.
4 E. S. Place, N. D. Evans and M. M. Stevens, *Nat. Mater.*, 2009, **8**, 457–470.
5 G. Fernandez de Grado, L. Keller, Y. Idoux-Gillet, Q. Wagner, A.-M. Musset, N. Benkirane-Jessel, F. Bornert and D. Offner, *J. Tissue Eng.*, 2018, **9**, 204173141877681.
6 S. Pina, J. M. Oliveira and R. L. Reis, *Adv. Mater.*, 2015, **27**, 1143–1169.
7 C. Gao, S. Peng, P. Feng and C. Shuai, *Bone Res.*, 2017, **5**, 17059.
8 J. M. Holzwarth and P. X. Ma, *Biomaterials*, 2011, **32**, 9622–9629.
9 D.-X. Wei, J.-W. Dao and G.-Q. Chen, *Adv. Mater.*, 2018, **30**, 1802273.
10 C. Zhu, S. Pongkitwitoon, J. Qiu, S. Thomopoulos and Y. Xia, *Adv. Mater.*, 2018, **30**, 1707306.
11 C. Zhu, J. Qiu, S. Pongkitwitoon, S. Thomopoulos and Y. Xia, *Adv. Mater.*, 2018, **30**, 1706706.
12 J. H. Jordahl, L. Solorio, H. Sun, S. Ramcharan, C. B. Teeple, H. R. Haley, K. J. Lee, T. W. Eyster, G. D. Luker, P. H. Krebsbach and J. Lahann, *Adv. Mater.*, 2018, **30**, 1707196.
13 K. Markstedt, A. Mantas, I. Tournier, H. Martínez Ávila, D. Hägg and P. Gatenholm, *Biomacromolecules*, 2015, **16**, 1489–1496.
14 J. G. Torres-Rendon, T. Femmer, L. De Laporte, T. Tigges, K. Rahimi, F. Gremse, S. Zafarnia, W. Lederle, S. Ifuku, M. Wessling, J. G. Hardy and A. Walther, *Adv. Mater.*, 2015, **27**, 2989–2995.
15 Q. Chen, R. P. Garcia, J. Munoz, U. Pérez de Larraya, N. Garmendia, Q. Yao and A. R. Boccaccini, *ACS Appl. Mater. Interfaces*, 2015, **7**, 24715–24725.
16 J. Song, C. Chen, S. Zhu, M. Zhu, J. Dai, U. Ray, Y. Li, Y. Kuang, Y. Li, N. Quispe, Y. Yao, A. Gong, U. H. Leiste, H. A. Bruck, J. Y. Zhu, A. Vellore, H. Li, M. L. Minus, Z. Jia, A. Martini, T. Li and L. Hu, *Nature*, 2018, **554**, 224–228.
17 H. Zhu, S. Zhu, Z. Jia, S. Parvinian, Y. Li, O. Vaaland, L. Hu and T. Li, *Proc. Natl. Acad. Sci. U. S. A.*, 2015, **112**, 8971–8976.
18 C. Chen and L. Hu, *Acc. Chem. Res.*, 2018, **51**, 3154–3165.
19 I. Usov, G. Nyström, J. Adamcik, S. Handschin, C. Schütz, A. Fall, L. Bergström and R. Mezzenga, *Nat. Commun.*, 2015, **6**, 7564.
20 B. D. Mattos, B. L. Tardy and O. J. Rojas, *Biomacromolecules*, 2019, **20**, 2657–2665.
21 N. Lavoine and L. Bergström, *J. Mater. Chem. A*, 2017, **5**, 16105–16117.
22 D. A. Osorio, B. E. J. Lee, J. M. Kwiecien, X. Wang, I. Shahid, A. L. Hurley, E. D. Cranston and K. Grandfield, *Acta Biomater.*, 2019, **87**, 152–165.
23 H. Autefage, F. Allen, H. M. Tang, C. Kallepitis, E. Gentleman, N. Reznikov, K. Nitiputri, A. Nommeots-Nomm, M. D. O'Donnell, C. Lange, B. M. Seidt, T. B. Kim, A. K. Solanki, F. Tallia, G. Young, P. D. Lee, B. F. Pierce, W. Wagermaier, P. Fratzl, A. Goodship, J. R. Jones, G. Blunn and M. M. Stevens, *Biomaterials*, 2019, **209**, 152–162.
24 L. Souza, J. H. Lopes, D. Encarnação, I. O. Mazali, R. A. Martin, J. A. Camilli and C. A. Bertran, *Sci. Rep.*, 2018, **8**, 12808.
25 I. D. Xynos, A. J. Edgar, L. D. K. Buttery, L. L. Hench and J. M. Polak, *Biochem. Biophys. Res. Commun.*, 2000, **276**, 461–465.

26 J. Zhang, H. Wu, F. He, T. Wu, L. Zhou and J. Ye, *Mater. Sci. Eng., C*, 2019, **99**, 1199–1212.
27 J. Kentleach, D. Kaigler, Z. Wang, P. Krebsbach and D. Mooney, *Biomaterials*, 2006, **27**, 3249–3255.
28 L. Liu, Y. Liu, C. Feng, J. Chang, R. Fu, T. Wu, F. Yu, X. Wang, L. Xia, C. Wu and B. Fang, *Biomaterials*, 2019, **192**, 523–536.
29 I. Roohaniesfahani, J. Wang, Y. J. No, C. de Candia, X. Miao, Z. Lu, J. Shi, D. L. Kaplan, X. Jiang and H. Zreiqat, *Mater. Sci. Eng., C*, 2019, **94**, 976–987.
30 L. Xu, R. Willumeit-Römer and B. J. C. Luthringer-Feyerabend, *Acta Biomater.*, 2019, DOI: 10.1016/j.actbio.2019.02.018.
31 W. Chen, H. Yu, S.-Y. Lee, T. Wei, J. Li and Z. Fan, *Chem. Soc. Rev.*, 2018, **47**, 2837–2872.
32 O. Nechyporchuk, M. N. Belgacem and F. Pignon, *Biomacromolecules*, 2016, **17**, 2311–2320.
33 H. Fan, C. Hartshorn, T. Buchheit, D. Tallant, R. Assink, R. Simpson, D. J. Kissel, D. J. Lacks, S. Torquato and C. J. Brinker, *Nat. Mater.*, 2007, **6**, 418–423.
34 H. Cai, S. Sharma, W. Liu, W. Mu, W. Liu, X. Zhang and Y. Deng, *Biomacromolecules*, 2014, **15**, 2540–2547.
35 F. J. O'Brien, *Mater. Today*, 2011, **14**, 88–95.
36 M. O. Wang, C. E. Vorwald, M. L. Dreher, E. J. Mott, M.-H. Cheng, A. Cinar, H. Mehdizadeh, S. Somo, D. Dean, E. M. Brey and J. P. Fisher, *Adv. Mater.*, 2015, **27**, 138–144.
37 B. D. Mattos, L. G. Greca, B. L. Tardy, W. L. E. Magalhães and O. J. Rojas, *Small*, 2018, **14**, 1–10.
38 H.-W. Kim, J.-H. Song and H.-E. Kim, *Adv. Funct. Mater.*, 2005, **15**, 1988–1994.
39 A. Hofmann, U. Ritz, S. Verrier, D. Eglin, M. Alini, S. Fuchs, C. J. Kirkpatrick and P. M. Rommens, *Biomaterials*, 2008, **29**, 4217–4226.
40 S. Verrier, M. Alini, E. Alsberg, S. Buchman, K. Kelly, M. Laschke, M. Menger, W. Murphy, J. Stegemann, M. Schütz, T. Miclau, M. Stoddart and C. Evans, *Eur. Cells Mater.*, 2016, **32**, 87–110.
41 H. A. Rather, D. Jhala and R. Vasita, *Mater. Sci. Eng., C*, 2019, **103**, 109761.
42 T. Kurobane, Y. Shiwaku, T. Anada, R. Hamai, K. Tsuchiya, K. Baba, M. Iikubo, T. Takahashi and O. Suzuki, *Acta Biomater.*, 2019, **88**, 514–526.
43 R. Núñez-Toldrà, S. Montori, B. Bosch, L. Hupa, M. Atari and S. Miettinen, *Tissue Eng., Part A*, 2019, DOI: 10.1089/ten.tea.2018.0256.
44 M. W. Laschke, A. Strohe, C. Scheuer, D. Eglin, S. Verrier, M. Alini, T. Pohlemann and M. D. Menger, *Acta Biomater.*, 2009, **5**, 1991–2001.
45 O. Oliviero, M. Ventre and P. A. Netti, *Acta Biomater.*, 2012, **8**, 3294–3301.
46 A. Artel, H. Mehdizadeh, Y.-C. Chiu, E. M. Brey and A. Cinar, *Tissue Eng., Part A*, 2011, **17**, 2133–2141.
47 J. H. Holstein, M. Orth, C. Scheuer, A. Tami, S. C. Becker, P. Garcia, T. Histing, P. Mörsdorf, M. Klein, T. Pohlemann and M. D. Menger, *Bone*, 2011, **49**, 1037–1045.
48 R. E. Geuze, L. F. H. Theyse, D. H. R. Kempen, H. A. W. Hazewinkel, H. Y. A. Kraak, F. C. Öner, W. J. A. Dhert and J. Alblas, *Tissue Eng., Part A*, 2012, **18**, 2052–2062.
49 L. Hench and J. Wilson, *Science*, 1984, **226**, 630–636.
50 T. A. Owen, M. Aronow, V. Shalhoub, L. M. Barone, L. Wilming, M. S. Tassinari, M. B. Kennedy, S. Pockwinse, J. B. Lian and G. S. Stein, *J. Cell. Physiol.*, 1990, **143**, 420–430.
51 K. Ibaraki, J. D. Termine, S. W. Whitson and M. F. Young, *J. Bone Miner. Res.*, 2009, **7**, 743–754.
52 O. Tsigkou, J. R. Jones, J. M. Polak and M. M. Stevens, *Biomaterials*, 2009, **30**, 3542–3550.
53 I. D. Xynos, A. J. Edgar, L. D. K. Buttery, L. L. Hench and J. M. Polak, *J. Biomed. Mater. Res.*, 2001, **55**, 151–157.
54 Y. Cai, H. Pan, X. Xu, Q. Hu, L. Li and R. Tang, *Chem. Mater.*, 2007, **19**, 3081–3083.
55 J. Ryu, S. H. Ku, H. Lee and C. B. Park, *Adv. Funct. Mater.*, 2010, **20**, 2132–2139.
56 P. X. Ma, *Adv. Drug Delivery Rev.*, 2008, **60**, 184–198.
57 C. M. Cowan, Y.-Y. Shi, O. O. Aalami, Y.-F. Chou, C. Mari, R. Thomas, N. Quarto, C. H. Contag, B. Wu and M. T. Longaker, *Nat. Biotechnol.*, 2004, **22**, 560–567.
58 J.-H. Ye, Y.-J. Xu, J. Gao, S.-G. Yan, J. Zhao, Q. Tu, J. Zhang, X.-J. Duan, C. A. Sommer, G. Mostoslavsky, D. L. Kaplan, Y.-N. Wu, C.-P. Zhang, L. Wang and J. Chen, *Biomaterials*, 2011, **32**, 5065–5076.
59 P. P. Spicer, J. D. Kretlow, S. Young, J. A. Jansen, F. K. Kasper and A. G. Mikos, *Nat. Protoc.*, 2012, **7**, 1918–1929.
60 Z. S. Patel, S. Young, Y. Tabata, J. A. Jansen, M. E. K. Wong and A. G. Mikos, *Bone*, 2008, **43**, 931–940.
61 S. Bose, M. Roy and A. Bandyopadhyay, *Trends Biotechnol.*, 2012, **30**, 546–554.
62 B. D. Boyan, E. M. Lotz and Z. Schwartz, *Tissue Eng., Part A*, 2017, **23**, 1479–1489.
63 Z. Schwartz, C. H. Lohmann, J. Oefinger, L. F. Bonewald, D. D. Dean and B. D. Boyan, *Adv. Dent. Res.*, 1999, **13**, 38–48.
64 P. Carmeliet, *Nature*, 2005, **438**, 932–936.
65 M. W. Laschke and M. D. Menger, *Biotechnol. Adv.*, 2016, **34**, 112–121.
66 X. Yu, E. A. Botchwey, E. M. Levine, S. R. Pollack and C. T. Laurencin, *Proc. Natl. Acad. Sci. U. S. A.*, 2004, **101**, 11203–11208.
67 N. J. Lakhkar, I.-H. Lee, H.-W. Kim, V. Salih, I. B. Wall and J. C. Knowles, *Adv. Drug Delivery Rev.*, 2013, **65**, 405–420.
68 A. Hoppe, N. S. Güldal and A. R. Boccaccini, *Biomaterials*, 2011, **32**, 2757–2774.
69 V. S. Salazar, L. W. Gamer and V. Rosen, *Nat. Rev. Endocrinol.*, 2016, **12**, 203–221.
70 V. Rosen, *Cytokine Growth Factor Rev.*, 2009, **20**, 475–480.

71 K. Schmidt-Bleek, B. M. Willie, P. Schwabe, P. Seemann and G. N. Duda, *Cytokine Growth Factor Rev.*, 2016, **27**, 141–148.
72 M. T. Islam, R. M. Felfel, E. A. Abou Neel, D. M. Grant, I. Ahmed and K. M. Z. Hossain, *J. Tissue Eng.*, 2017, **8**, 1–16.
73 T. Winkler, F. A. Sass, G. N. Duda and K. Schmidt-Bleek, *Bone Joint Res.*, 2018, **7**, 232–243.
74 W. Li, N. Garmendia, U. Pérez de Larraya, Y. Ding, R. Detsch, A. Grünewald, J. A. Roether, D. W. Schubert and A. R. Boccaccini, *RSC Adv.*, 2014, **4**, 56156–56164.
75 N. Ashammakhi, A. Hasan, O. Kaarela, B. Byambaa, A. Sheikhi, A. K. Gaharwar and A. Khademhosseini, *Adv. Healthcare Mater.*, 2019, 1801048.